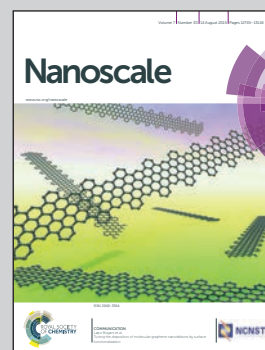


Showcasing research from the Wuhan Institute of Physics and Mathematics, Chinese Academy of Sciences, Wuhan, China.

MRI-visible liposome nanovehicles for potential tumor-targeted delivery of multimodal therapies

A multifunctional liposome possessing both MRI-visible and therapeutic features was developed to overcome the insolubility of paclitaxel, reduce the side effects of the FDA-approved formulation of PTX-Cre (Taxol®) and improve drug delivery efficiency to the tumor. The delivery system provides a minimally invasive and real-time MRI strategy with enhanced sensitivity over non-targeted delivery vehicles.

As featured in:



See Xin Zhou et al.  
*Nanoscale*, 2015, 7, 12843.



[www.rsc.org/nanoscale](http://www.rsc.org/nanoscale)

Registered charity number: 207890



Cite this: *Nanoscale*, 2015, 7, 12843

## MRI-visible liposome nanovehicles for potential tumor-targeted delivery of multimodal therapies

Lili Ren, Shizhen Chen, Haidong Li, Zhiying Zhang, Chaochui Ye, Maili Liu and Xin Zhou\*

Real-time diagnosis and monitoring of disease development, and therapeutic responses to treatment, are possible by theranostic magnetic resonance imaging (MRI). Here we report the synthesis of a multifunctional liposome, which contains Gd-DOTA (an MRI probe), paclitaxel and c(RGDyK) (a targeted peptide). This nanoparticle overcame the insolubility of paclitaxel, reduced the side effects of FDA-approved formulation of PTX-Cre (Taxol®) and improved drug delivery efficiency to the tumor. c(RGDyK) modification greatly enhanced the cytotoxicity of the drug in tumor cells A549. The  $T_1$  relaxivity in tumor cells treated with the targeted liposome formulation was increased 16-fold when compared with the non-targeted group. *In vivo*, the tumors in mice were visualized using  $T_1$ -weighted imaging after administration of the liposome. Also the tumor growth could be inhibited well after the treatment. Fluorescence images *in vitro* and *ex vivo* also showed the targeting effect of this liposome in tumor cells, indicating that this nanovehicle could limit the off-target side effects of anticancer drugs and contrast agents. These findings lay the foundation for further tumor inhibition study and application of this delivery vehicle in cancer therapy settings.

Received 3rd April 2015,

Accepted 7th May 2015

DOI: 10.1039/c5nr02144h

www.rsc.org/nanoscale

### Introduction

Liposomes, consisting of a 5 nm thick lipid bilayer shell surrounding an aqueous core, are the most clinically established nanoscale systems used to deliver cytotoxic and antifungal drugs, genes, vaccines, as well as imaging agents.<sup>1–12</sup> Biocompatibility, biodegradability, reduced toxicity, and capacity for size and surface manipulations comprise the outstanding profile that liposomes offer over other delivery systems. As drug carriers, liposomes have successfully encapsulated different therapeutic drugs, including doxorubicin,<sup>12,13</sup> platinum anticancer drugs,<sup>5,14</sup> cathepsin protease inhibitor,<sup>3</sup> irinotecan,<sup>15</sup> vinorelbine, parthenolide,<sup>16</sup> and diclofenac sodium.<sup>17</sup> Paclitaxel, which is water insoluble and difficult to modify, can be successfully loaded in liposomes to improve the therapy outcome.<sup>18</sup> Gd-chelates (Gd-DOTA/Gd-DTPA) have been widely applied in clinical diagnosis for their safety and positive magnetic resonance imaging (MRI) contrast.<sup>19–22</sup> As a contrast agent, Gd-chelate-encapsulated liposomes allowed significant contrast evaluation of drug efficacy in the tumor.<sup>1,8,19–21</sup>

Theranostics is a term that defines ongoing efforts to develop more specific, bespoke therapies for various diseases and combine these with diagnostic properties into a single pharmaceutical agent.<sup>20,23,24</sup> As the field of molecular imaging has emerged from the blending of molecular biology with medical imaging, liposomes are increasingly common for both therapeutic and diagnostic applications.<sup>10,20,21</sup> Diagnosis and therapy are traditionally regarded as two separate issues in medical care. To achieve an optimal curative effect for many diseases, especially in cancer, they have been combined mutually and synergistically. Theranostic liposomes provide a feasible approach to accurately locate the tumor tissues and monitor the drug behavior and therapeutic responses to individual treatments.<sup>1,3,8,19,25</sup>

To further decrease the side effects and improve the accumulation of the drug and contrast agents in the tumor, a group selective for cancer cells is needed.<sup>4–12</sup> Integrin, overexpressed in many solid tumor cells, has a direct effect in preventing apoptosis in cancer cells and mediating proangiogenic interactions between endothelial cells and the extracellular matrix.<sup>21,26–29</sup> Peptides with arginine-glycine-aspartic acid (RGD) sequences are known to bind to integrin receptors with high affinity. Probes with RGD peptides have been used to image  $\alpha_v\beta_3$  integrin receptor expression and related objects by fluorescence, MRI, PET or other techniques.<sup>17,27,30</sup> A cyclic targeted peptide, c(RGDyK), has a higher binding affinity and specificity than linear peptides or multimers of the RGD

Key Laboratory of Magnetic Resonance in Biological Systems, State Key Laboratory of Magnetic Resonance and Atomic and Molecular Physics, National Center for Magnetic Resonance in Wuhan, Wuhan Institute of Physics and Mathematics, Chinese Academy of Sciences, Wuhan 430071, China. E-mail: xinzhou@wipm.ac.cn; Fax: +86-27-8719-9291; Tel: +86-027-8719-8802

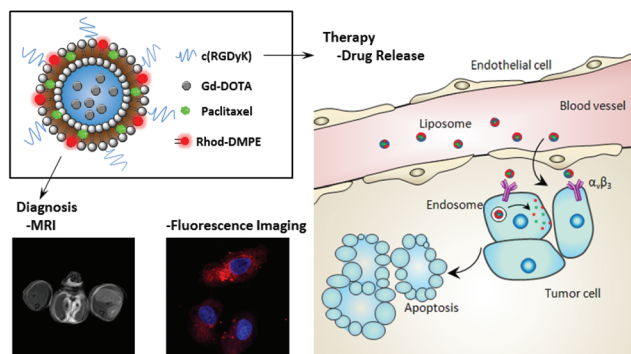


**Fig. 1** Schematic of the structure of the multifunctional liposome and the application of this liposome in theranostics. The nanoprobes can be internalized and activated by  $\alpha_v\beta_3$ -mediated endocytosis in tumor cells. The drug and the contrast agent can be released after the destabilization of the endosome provoked by the liposome, thus realizing targeted imaging and tumor therapy.<sup>5,9,27,31,35</sup>

peptide.<sup>18,31–34</sup> As illustrated in Fig. 1, nanoparticles with RGD peptides can be internalized into tumor cells and release substances to treat cancer and enhance the tumor signal.<sup>5,9,27,31,35</sup>

The work presented here addresses the development of an effective approach for the preparation of a theranostic liposome, which contains paclitaxel in the bilayer for cancer drug treatment, a targeted group, c(RGDyK), and Gd-DOTA as the  $T_1$  contrast agent for MRI-visible enhancement for non-small-cell lung cancer cell, A549 ( $\alpha_v\beta_3$  integrin positive cell<sup>27–29</sup>). Liposomes were also labeled with rhodamine for detection by fluorescence imaging. The behavior of this theranostic nanoprobe was detected *in vitro* and *in vivo*. These bifunctional liposomes, possessing both MRI-visible and therapeutic potential, may hold promise as theranostic agents for multimodal nanomedicine, owing to the properties such as high sensitivity, deep tissue penetration and good anticancer efficiency.

## Experimental

### Chemicals

1,2-Distearoyl-*sn*-glycero-3-phosphocholine (DSPC), 1,2-distearoyl-*sn*-glycero-3-phosphoglycerol sodium salt (DSPG-Na) and *N*-(carbonyl-methoxypolyethyleneglycol-2000)-1,2-distearoyl-*sn*-glycero-3-phosphoethanolamine, sodium salt (MPEG-2000-DSPE) were purchased from Cordon Pharma. *N*-(Carboxy-polyethyleneglycol-2000)-1,2-distearoyl-*sn*-glycero-3-phosphoethanolamine, ammonium salt (COOH-PEG2000-DSPE) was purchased from Nanocs. 1,2-Dimyristoyl-*sn*-glycero-3-phosphoethanolamine-*N*-(lissamine rhodamine B sulfonyl), ammonium salt (Rhod-DMPE) was purchased from Avanti Polar lipids. DOTA was purchased from Strem Chemicals. GdCl<sub>3</sub> was purchased from Sigma-Aldrich. c(RGDyK) was obtained from GL Bioche. Paclitaxel was obtained from Shuanye. All other reagents were of analytical grade.

### Preparation of paclitaxel-contrast agent-loaded and fluorescence-labeled liposomes

The liposome composed of DSPC, DSPG, and MPEG-2000-DSPE at 7 : 2 : 1 (mol) was prepared by a thin film hydration method, followed by membrane extrusion.<sup>5,12,15,16</sup> Briefly, 15 mg of lipids were dissolved in 1 mL chloroform/methanol/water (1 : 1 : 0.3, v/v/v) and dried under vacuum to form a film. The resulting lipid film was then placed under high vacuum overnight and hydrated with PBS (pH 7.4) by sonication in a water bath for 10 min. The blank liposome was obtained.

For a PTX-contrast agent-loaded liposome (Gd-PTX-L), PTX was added to the lipid solution at a molar ratio of 1 : 30 (drug : lipid). The lipid film was formed by evaporation using a rotary evaporator. The film was then hydrated with 1 mL aqueous solution of 150 mM DOTA/100 mM GdCl<sub>3</sub> (pH 3.5) to form multilamellar vesicles. These vesicles were sonicated for 10 min and subsequently extruded 10 times through polycarbonate filters, 0.2  $\mu$ m pore size, by using an Avanti mini-extruder. Non-encapsulated PTX was removed by centrifuging for 10 min at 2000 rpm. The exterior buffer of the liposome was exchanged by PBS (pH 7.4) *via* dialysis (10 kDa) for 4 h.<sup>1,4,36</sup>

To form the targeted liposome (RGD-Gd-PTX-L), the peptide-lipid conjugate c(RGDyK)-PEG2000-DSPE was synthesized.<sup>37,38</sup> COOH-PEG2000-DSPE was dissolved in PBS buffer. Appropriate amounts of *N*-hydroxysuccinimide (NHS) and 1-(3-dimethylaminopropyl)-3-ethyl carbodiimide hydrochloride (EDCI) were added to the solution. After incubation at room temperature for 30 min, c(RGDyK) was added and incubated for 10 h. Excess unreacted peptides were removed by dialysis (2000 Da). The conjugate was then lyophilized for the subsequent procedures. The molar ratio was 7 : 2 : 1 : 0.5 of DSPC, DSPG, MPEG-2000-DSPE and c(RGDyK)-PEG2000-DSPE. Targeted liposome preparation was the same as that of Gd-PTX-L.

Rhodamine-labeled liposome (Rh-L) was composed of DSPC, DSPG, MPEG-2000-DSPE and Rhod-DMPE at a molar ratio of 7 : 2 : 1 : 0.2. Rhod-DMPE was dissolved in the organic phase. The fluorescent liposome was prepared by the same method as above.<sup>1,6,37</sup> The whole process was protected from light.

The resulting liposomes were characterized using dynamic light scattering (DLS) with a zetasizer nano ZS (Malvern, England) for hydrodynamic diameter and zeta potential determination, and transmission electron microscopy (TEM) by Tecnai G20 (FEI, USA).

### Quantification of encapsulated PTX and Gd

The content of PTX incorporated into liposomes was detected by HPLC (Agilent, USA). The liposomes were diluted by the addition of water and acetonitrile to a total volume of 0.5 mL. PTX was extracted by the addition of 4.0 mL of *tert*-butyl methyl ether and mixing for 30 s. The mixture was centrifuged for 15 min at 300 *g*, after which 3 mL of the organic layer was transferred and evaporated. The residue was dissolved in 100  $\mu$ L of a 7/3 acetonitrile/water mixture. 50  $\mu$ L of this solu-

tion was injected into a C<sub>18</sub> column guard. The flow rate was 1.0 mL min<sup>-1</sup>; the detection wavelength was set at 227 nm. The drug concentration was calculated from standard curves. The assay was linear over the concentration range from 1 µg to 500 µg.<sup>4,39</sup>

The Gd content of the liposomes was determined by ICP-MS (Thermo, USA).<sup>14</sup> A sample volume of 0.25 mL was diluted with 0.5 mL water. After addition of 1.5 mL HNO<sub>3</sub>, the sample was heated to approximately 100 °C for 30 min, then diluted to 50 mL with water.<sup>40</sup> Calibration was done with a Gd ICP standard solution. The encapsulation efficiency was calculated according to eqn (1), in which PTX(Gd)<sub>final</sub> is the content of PTX or Gd in the liposome and PTX(Gd)<sub>total</sub> is the original content added to the lipid.

$$\text{encapsulation efficiency(\%)} = \frac{\text{PTX(Gd)}_{\text{final}}}{\text{PTX(Gd)}_{\text{total}}} \times 100\% \quad (1)$$

### Physical stability of liposomes

The physical stability of RGD-Gd-PTX-L was evaluated under the storage conditions (in PBS) at 4 °C or in fetal bovine serum (liposome : serum = 1 : 2, v/v) at 37 °C. Certain amounts of samples were taken from the pool at different times. The samples were centrifuged for 15 min at 300×g. The following PTX extraction and detection were the same as the content of PTX above. The released drug can be calculated compared to the original content of PTX in the liposome.<sup>39</sup>

### Fluorescence microscopy studies of the targeted liposomes

Non-small-cell lung cancer cell A549 and human normal lung fibroblast cell WI-38 (1 × 10<sup>5</sup> cells) were seeded on cover slips placed in a cell culture dish and cultured in IMDM (Iscove's modified Dulbecco's medium, Boster, China) and MEM (minimum essential medium, Boster, China) respectively, supplemented with 10% fetal bovine serum (Boster, China), 100 U mL<sup>-1</sup> penicillin and streptomycin (Boster, China) under humidified air with 5% CO<sub>2</sub> at 37 °C. The regular culture media were removed when the cell confluence reached 30%–40%. IMDM and MEM media containing the rhodamine-labeled liposome were added. After 4 h of incubation at 37 °C, the cells were fixed with 4% paraformaldehyde, and then incubated with DAPI for 5 min. All cells were washed at least three times with PBS. The fluorescence images were recorded on a confocal laser scanning microscope (CLSM, Nikon, Japan).<sup>4,5</sup>

### In vitro cytotoxicity assays

Approximately 1 × 10<sup>4</sup> cells were seeded per well in 96-well plates and cultured for 24 h. RGD-Gd-PTX-L, Gd-PTX-L, blank liposomes and PTX (dissolved in cremophor/ethanol, 50 : 50, v/v) were diluted in IMDM/MEM media and added to the wells, respectively. After 4 h of incubation, the cells were then cultured in regular culture medium for 2 days. MTT was added to the culture medium at a concentration of 0.5 mg mL<sup>-1</sup> during the last 4 h of the culture. The medium was carefully removed and 200 µL DMSO was added per well. The optical density at

490 nm for each well was measured by using an ELISA plate reader (Molecular Devices, USA).<sup>5,34,41</sup> The 50% inhibitory concentration (IC<sub>50</sub>) was graphically calculated from concentration–effect curves, considering the optical density of the control well as 100%.

### Cellular uptake study

The cells (1 × 10<sup>6</sup> cells) were cultured in 25 mL cell culture flasks until >90% confluence was reached. After 4 h of incubation with RGD-Gd-PTX-L and Gd-PTX-L (containing 20 µg paclitaxel each), the cells were harvested using 1% triton to destroy any cell pellets.<sup>41</sup> The extraction and detection methods of PTX were the same as detailed for the quantification of PTX. The cellular uptake efficiency was calculated using eqn (2), in which PTX<sub>cell</sub> is the content of PTX inside the cell and PTX<sub>lipo</sub> is the content inside the liposome.

$$\text{cellular uptake efficiency(\%)} = \frac{\text{PTX}_{\text{cell}}}{\text{PTX}_{\text{lipo}}} \times 100\% \quad (2)$$

### In vitro MR contrast properties of the liposomes

The cell culture process was the same as the cellular uptake study. When the cell confluence was greater than 90%, the targeted liposome (RGD-Gd-PTX-L) and the control group (Gd-PTX-L) were diluted with IMDM/MEM to differing concentrations of Gd and then added to the flasks. After 4 h of incubation, cells were washed at least three times to remove any unbound liposomes and harvested with 500 µL H<sub>2</sub>O/D<sub>2</sub>O (2 : 98, v/v).<sup>41</sup>

The MR contrast effect of this liposome was examined by measuring the proton longitudinal relaxation time (T<sub>1</sub>) of the cell solution, which refers to the longitudinal relaxation rate (1/T<sub>1</sub>) in the presence of paramagnetic substances. All the samples were detected by using a 500 MHz NMR analyzer (Bruker, USA) with a standard inversion-recovery pulse sequence. Furthermore, 250 µL of the samples added to 96 well plates were imaged using a 7 T MRI scanner with a spin-echo method (TR = 500 ms; TE = 11 ms; FOV = 8 × 8 cm; 10 mm slice thickness) (Bruker, USA).<sup>1,14,40</sup>

### In vivo MR contrast properties of the liposomes

BALB/c male nude mice (aged 5–6 weeks, approx. 20 g) were inoculated subcutaneously in the legs with A549 cells (1 × 10<sup>6</sup> cells in 250 µL PBS) and examined using MRI 3 weeks after inoculation. 7 T MRI monitored the liposomes, which were gathering in tumor-bearing mice, by repeated scanning prior to treatment (for baseline evaluation) and post-treatment. Tumor-bearing mice were oriented in the prone position. The mice were initially anesthetized with 3% isoflurane and then 1% isoflurane using a gas controller (Matrx, USA). The respiratory cycle was monitored using a pneumatic pillow. T<sub>1</sub> was measured using a saturation-recovery technique, involving acquisition of T<sub>1</sub>-weighted MR images before and after administration of the liposome *via* the tail vein, using a spin echo technique (TE = 11 ms; TR = 120, 150, 180, 200, 300, 500, 800, 1200, 2000, 3000, 5000 ms; 1 mm slice thickness; 22 min data

acquisition; RARE factor = 1; matrix size =  $256 \times 256$ , FOV =  $4 \times 4$  cm).<sup>1,14</sup> Image analysis was performed by using ParaVision 5.0.

For the *ex vivo* study, rhodamine-labeled liposome (Rh-RGD-Gd-PTX-L) was injected intravenously (i.v.) into the A549-grafted mouse model. After 1 h administration, the tumor was resected, fixed in 10% paraformaldehyde overnight, dehydrated by 30% sucrose and molded with paraffin or frozen for section. The sections were cut to a 20  $\mu\text{m}$  thickness and stained with DAPI for fluorescence imaging by CLSM. The sections were cut to 10  $\mu\text{m}$  and stained with haematoxylin and eosin for histological analysis.<sup>3</sup>

### *In vivo* tumor inhibition effect

Tumor inhibition effect of RGD-Gd-PTX-L was evaluated by using a 7 T MRI scanner. The fixation and anesthesia processes were the same as above. 200  $\mu\text{L}$  liposome was injected *via* the tail vein. The control group was injected with the same volume of saline. The liposome and saline were injected on days 0, 2, 4, 7, 10, 14 and 16. The MRIs were taken on days 0, 10 and 23 with the same parameters as before. When taking the MRIs of the control group, the same amount of RGD-Gd-L was applied.  $T_1$ -weighted MRIs were obtained 1 h after the administration of the contrast agent-loaded liposome. Image analysis was performed by using ParaVision 5.0. Regions of interest were identified using a mouse atlas of anatomy. The tumor volume was estimated as the sum of the tumor volume of all slices.<sup>1,4</sup>

## Results and discussion

### Characterization

The structure of the multifunctional liposome is illustrated in Fig. 1. Liposomes are composed of lipid molecules that self-assemble into a hollow double-layered sphere, into which PTX and Gd-DOTA are inserted. The targeted ligand c(RGDyK) is covalently conjugated to the liposome. This liposome can be delivered to the tumor site and release anticancer drugs and contrast agents *in vivo*. TEM images provide evidence for the round shape of these particles with mean diameters around 162 nm, as detected by DLS (Fig. 2A). The drug release rate was 1.5% after 2 days of storing in PBS at 4  $^{\circ}\text{C}$  and 46.84% in serum at 37  $^{\circ}\text{C}$  (Fig. 2B), indicating the good physical stability of RGD-Gd-PTX-L under storage conditions and relatively slow drug release in serum. The high drug release rate in serum may relate to the high temperature and serum protein. High temperature may speed up the release of drug from the liposome. Also the liposome structure would be changed by exposure to serum proteins.<sup>9,37,39</sup> The formulation parameters are listed in Table 1. The diameter of RGD-Gd-PTX-L was  $161.7 \pm 5.5$  nm. Approximately  $14.36 \pm 3.85\%$  of Gd-DOTA was loaded into the targeted liposome. The loading efficiency of PTX was  $71.10 \pm 4.73\%$ .

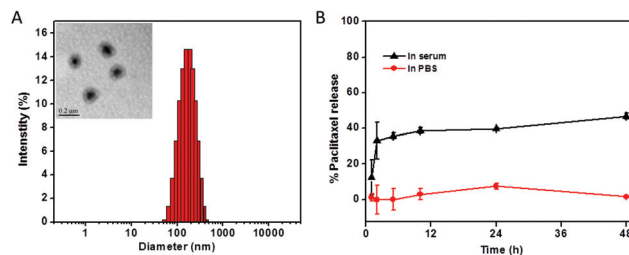


**Fig. 2** (A) DLS measurement of the corresponding liposome showing the distribution of diameters and the size (diameter = 162.2 nm). Inset: image of RGD-Gd-PTX-L by TEM shows the round-shape of the liposome. (B) *In vitro* release of paclitaxel from RGD-Gd-PTX-L under storage conditions at 4  $^{\circ}\text{C}$  or in serum at 37  $^{\circ}\text{C}$ . Data are presented as mean  $\pm$  SD,  $n = 3$ .

**Table 1** Formulation parameters. All data are presented as mean  $\pm$  standard deviation (SD),  $n = 3$

Group	Diameter (nm)	Zeta potential (mV)
RGD-Gd-PTX-L	$161.7 \pm 5.5$	$-7.97 \pm 3.99$
Blank L	$141.1 \pm 8.7$	$-5.79 \pm 1.27$

	Concentration	Entrapment efficiency (%)
Gd	$3.28 \pm 0.26$ mM	$14.36 \pm 3.85$
PTX	$0.12 \pm 0.04$ mg mL <sup>-1</sup>	$71.10 \pm 4.73$

### Tumor targeting by fluorescence analysis

To investigate the tumor targeting effect of c(RGDyK) modified liposome, lung cancer cell A549 and normal lung cell WI-38 were incubated with rhodamine-labeled RGD-Gd-PTX-L and Gd-PTX-L. Fig. 3A shows the fluorescence micrographs of different groups. For A549 cells, the red fluorescence (attributed to rhodamine) intensity in RGD-Gd-PTX-L-bound cells was distinguishably higher than that of Gd-PTX-L-bound cells. For WI-38 cells, the fluorescence intensity was quite low. The differences between groups of RGD-Gd-PTX-L and Gd-PTX-L were obvious. Also A549 cell absorption of liposomes could be clearly seen in different slices (Fig. 3B). Most liposomes were located in cytoplasm. Co-localization of red and blue indicated the presence of liposomes in nucleus. This phenomenon demonstrated receptor mediated endocytosis when the integrin receptor on the tumor cell specifically recognized the targeted liposome.<sup>5,27,31</sup> Overall, the fluorescence intensity was much higher in A549 cells than WI-38 cells. Thus this drug delivery system may decrease the side effects of PTX and improve the drug efficiency.<sup>5</sup>

### Cytotoxicity of liposomes and cellular uptake of PTX

To explore the improvement of drug action by the targeted cargo, cell-killing ability of different groups of liposomes was evaluated by the MTT assay. Blank liposomes had no significant effect on either cell lines (the data are not shown here). The results demonstrated the dose-dependent toxicity on A549

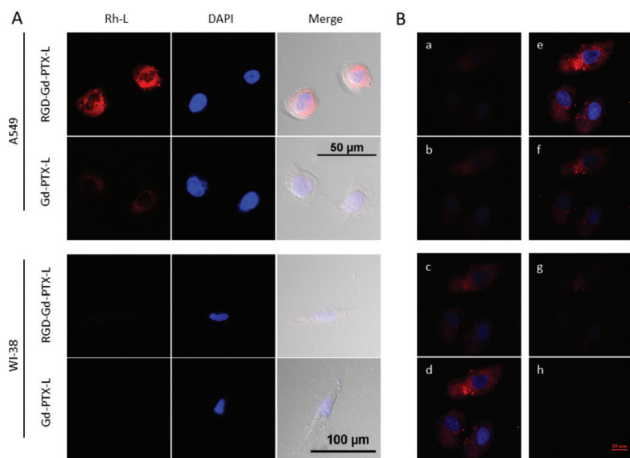


**Fig. 3** (A) Binding of rhodamine labeled liposomes (red) in tumor cell A549 and normal cell WI-38 by confocal laser scanning microscopy. A549 and WI-38 were treated with Rh-RGD-Gd-PTX-L and Rh-Gd-PTX-L at a PTX concentration of  $1 \mu\text{g mL}^{-1}$  for 4 h at  $37^\circ\text{C}$ . Cell nucleus was stained with DAPI (blue). (B) Internalization of targeted liposome (red) in A549 cells. Eight slices of fluorescence images from the top to the bottom (a to h) of the cells are shown using the Z-stack scan mode (step =  $2 \mu\text{m}$ ).

and WI-38 cells (Fig. 4A). Integrin is highly expressed in many cancer cells, and RGD peptides can target integrin and induce apoptosis.<sup>26</sup> When the concentration of PTX was  $16 \mu\text{g mL}^{-1}$ , the viability of A549 cells was approximately 38% and 75.4% for targeted and control groups, respectively. The cytotoxic effect of RGD-Gd-PTX-L and Gd-PTX-L on WI-38 was relatively low, even when the concentration of PTX was  $16 \mu\text{g mL}^{-1}$  (the cell viability was about 97.33% and 98.64%, respectively). Apoptotic response in A549 cells was much stronger than in WI-38 cells. RGD-Gd-PTX-L resulted in significantly higher toxicity than Gd-PTX-L for A549 cells, suggesting that c(RGDyK)-modified liposome decreased cell viability, resulting in a lower

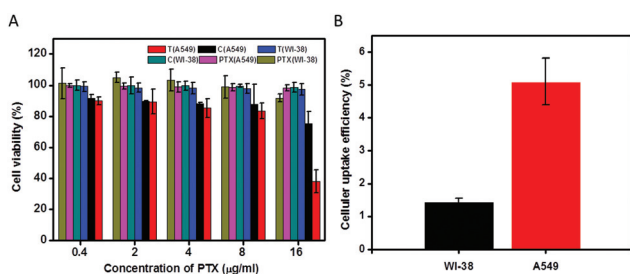


**Fig. 4** (A) Liposomal PTX drug efficacies in A549 and WI-38. PTX loaded liposomes and PTX were added into both cell lines at concentrations of 0.4, 2, 4, 8 and  $16 \mu\text{g mL}^{-1}$ . The resulting cytotoxicity was determined as a percentage of viable cells. RGD-Gd-PTX-L (T) and Gd-PTX-L (C) were the targeted and control liposomes respectively. Data are presented as mean  $\pm$  SD,  $n \geq 3$ . (B) Cellular uptake of RGD-Gd-PTX-L by A549 and WI-38. Data are presented as mean  $\pm$  SD,  $n = 3$ .

$\text{IC}_{50}$  ( $15 \mu\text{g mL}^{-1}$  and  $35 \mu\text{g mL}^{-1}$  of RGD-Gd-PTX-L and Gd-PTX-L, respectively in A549 cells).

In order to ascertain the exact amount of PTX internalized by A549 and WI-38 cells, PTX was extracted and then detected by HPLC. RGD-Gd-PTX-L showed an approximate 3.6-fold increase in uptake by A549 cells when compared to WI-38 cells under the same conditions (Fig. 4B). These results confirmed that this novel integrin-targeted-PTX-loaded liposome had low, non-specific toxicity and a more efficient antitumor effect than non-targeted equivalents.

### *In vitro* MR contrast enhancement of the targeted liposomes

The MR contrast properties of RGD-Gd-PTX-L were evaluated *in vitro* using A549 and WI-38 cell lines. The longitudinal relaxation times ( $T_1$ ) were measured using different concentrations of RGD-Gd-PTX-L and Gd-PTX-L. The baseline of longitudinal relaxation rates ( $1/T_1$ ) for the pre-treatment tumor cells was  $0.13 \pm 0.01 \text{ s}^{-1}$  at 500 MHz and then increased significantly after incubation with Gd-DOTA-loaded liposomes ( $4.03 \pm 0.04 \text{ s}^{-1}$  and  $2.95 \pm 0.03 \text{ s}^{-1}$  for the targeted and control groups, respectively, at a Gd concentration of  $0.6 \mu\text{M}$ ) (Fig. 5A).  $1/T_1$  of A549 cells decreased (for example,  $3.39 \pm 0.13 \text{ s}^{-1}$  for the targeted group) when the concentration of Gd was increased to  $1 \mu\text{M}$ . This might be related to the alteration of the cell structure and the function when treated with relatively high drug concentrations. The largest  $1/T_1$  of A549 cells incubated with the targeted liposome increased more than 30 times compared to that of A549 cells treated with non-targeted liposomes. As

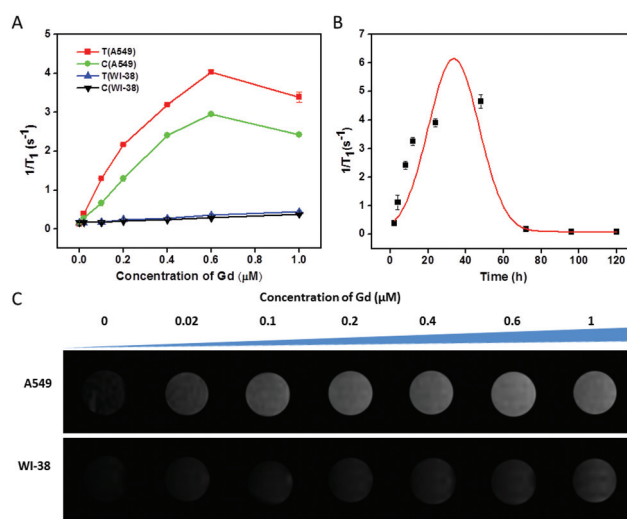


**Fig. 5** MR contrast properties of targeted liposomes. (A) Longitudinal relaxation rates ( $1/T_1$ ) of A549 and WI-38 incubated with Gd-DOTA-loaded liposomes detected by using a 500 MHz NMR analyzer. The concentrations of Gd were 1, 0.6, 0.4, 0.2, 0.1 and  $0.02 \mu\text{M}$  respectively. T represents RGD-Gd-PTX-L; C Gd-PTX-L. (B)  $1/T_1$  of A549 incubated with RGD-Gd-PTX-L at different times (PTX,  $26 \mu\text{g mL}^{-1}$ ; Gd,  $1 \mu\text{M}$ ) detected by using a 500 MHz NMR analyzer. (C)  $T_1$ -weighted MR images of A549 and WI-38 incubated with RGD-Gd-PTX-L at different concentrations corresponding to (A) detected by using a 7 T scanner. Data are presented as mean  $\pm$  SD,  $n = 3$ .

for WI-38 cells,  $1/T_1$  was increased gradually with the increase of the liposome concentration.  $1/T_1$  was  $0.44 \pm 0.02 \text{ s}^{-1}$  and  $0.38 \pm 0.01 \text{ s}^{-1}$  for the targeted and control groups, respectively, when the Gd concentration was  $1 \mu\text{M}$ . There was no significant difference in  $1/T_1$  between the targeted and control groups in WI-38 cells. Longitudinal relaxation enhancement of A549 cells was much larger than WI-38 cells, indicating the site-specific accumulation of liposomes in cancer cells.<sup>31</sup> The more the liposomes were internalized into cells the larger the longitudinal relaxation rate, and the greater the enhancement of the MRI signal. The  $1/T_1$  obtained by 7 T showed similar results as above (the data are not shown here).

The longitudinal relaxation times of tumor cells incubated with targeted liposomes for different periods were also investigated (Fig. 5B).  $1/T_1$  increased gradually when the incubation time was longer, peaking on day 2 ( $4.66 \pm 0.23 \text{ s}^{-1}$ ). It then dropped significantly on day 3 ( $0.18 \pm 0.01 \text{ s}^{-1}$ ).  $T_1$  relaxivity improved with the increasing Gd-DOTA, and then decreased when cell apoptosis started to occur. Thus, it is possible that the drug effect and tumor variation could be detected *in vivo* by MRI.

$T_1$  variation of tumor and normal cells incubated with liposomes could be visualized, as shown in Fig. 5C. The  $T_1$  signal improved gradually with the increasing concentration of Gd in both cell lines, with the exception of A549 cells when Gd was  $1 \mu\text{M}$  (the signal decreased). Briefly, the signal in A549 cells was much higher than that found in WI-38 cells under the same conditions. Furthermore, the signal from the targeted group was much higher than that of the control group. Compared to normal cells (WI-38), the tumor cells (A549) absorbed more liposomes. This can possibly be accounted for by the greater number of receptors on the tumor cell surface and/or the different behaviors of the cell lines.<sup>5</sup>

### Targeted liposome as the MRI-visible drug delivery system *in vivo*

As shown in Fig. 6A,  $T_1$  relaxation was significantly accelerated in the tumor after *i.v.* injection of liposome at a Gd concentration of  $8 \mu\text{M kg}^{-1}$ . The  $T_1$  baseline for the pre-treatment tumor was 1664 ms, which then decreased 44 min after administration of the targeted liposome (922 ms). Not only the rim, but also the core of the tumor turned bright. The decrease percentage of  $T_1$  was 44.59% and 43.61% respectively after 44 min or 1 h administration of the liposome. The contrast enhancement was much higher than some research studies.<sup>1,32</sup> The  $T_1$  relaxation enhancement was maintained for more than 4 h (Fig. 6B) and then returned to original levels after 1 day ( $T_1$  was 1600 ms at 24 h). No significant acute toxicity was recorded in the mouse during and after the test and the liposomal formulation of the PTX overcame the poor solubility of this drug, reducing dose-related side effects.<sup>4,18,39,42-44</sup> Also the contrast enhancement was relatively high for a long period, which may be related to the enhanced permeability and retention effect,<sup>14,18</sup> and the longer blood circulation time of the liposome provided by the PEG-lipid.<sup>1,18,39</sup> Collectively,

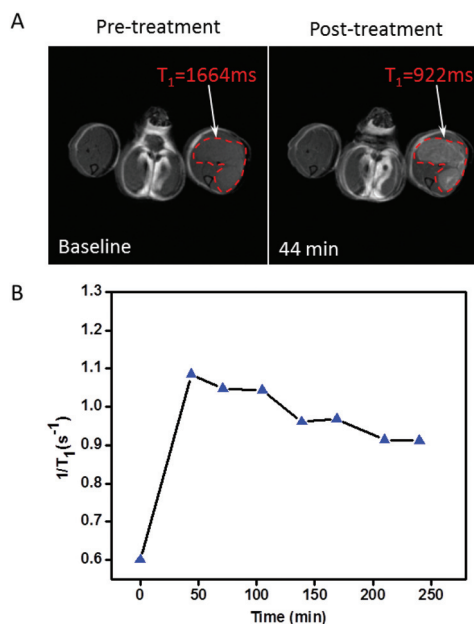


**Fig. 6** MRI analysis of the tumors before and after treatment with targeted liposomes. (A)  $T_1$ -weighted MR images of a mouse before and after the treatment with RGD-Gd-PTX-L. The tumor boundary is demarcated by the red dotted lines. The tumor volume was approximately  $5 \times 3 \text{ mm}$ . (B) Longitudinal relaxation rate ( $1/T_1$ ) variation of the tumor with the time after administration of the targeted liposome.

this particle has improved tumor targeting ability *via i.v.* administration, and monitoring by MRI.

To further study the targeting ability of the liposome *in vivo*, rhodamine-labeled liposome was injected into the cancer cell transplanted mouse. Fluorescence images were taken by CLSM after tissue sections were prepared. The liposome was successfully delivered to the tumor site (Fig. 7), not only inside the tumor (Fig. 7, inset), but also in the stroma whereas the normal cell absorbed very little liposomes. Combined with the tumor  $T_1$ -weighted MR images, the fluorescence results also showed the targeting effect of liposomes on the tumor site *in vivo*. Most importantly, the liposome could be identified in the tumor microenvironments. It is known that the tumor stroma is important for tumor progression.<sup>3,45</sup> This finding is promising for early cancer or tumor metastasis control.

The antitumor efficiency of this multifunctional liposome could be monitored by  $T_1$ -weighted MRIs (Fig. 8). Compared with the control group, the representative tumor images showed apparent tumor growth inhibition by RGD-Gd-PTX-L, especially at day 10 after the first week of intense drug administration. The tumor volumes of the liposome and saline groups were 8 and  $9 \text{ mm}^3$  before the treatment, and 17 and  $30 \text{ mm}^3$  after the treatment period, respectively. These results showed the potential of the liposomes in effective lung cancer treatment. Based on the preliminary studies, these liposomes could be involved in further applications, such as detecting

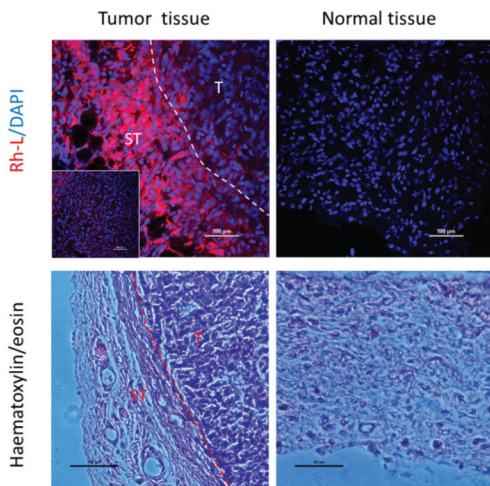


**Fig. 7** *Ex vivo* detection of the fluorescent-targeted liposome in the tumor. Representative fluorescent and hematoxylin & eosin staining images of tumor and normal tissues after injection of Rh-RGD-Gd-PTX-L (red). Insert: image of the inside tumor. Stromal (ST) and tumor (T) compartments of the tumor tissue are demarcated by the dotted line. Tumor volume was approximately  $3.5 \times 3$  mm.

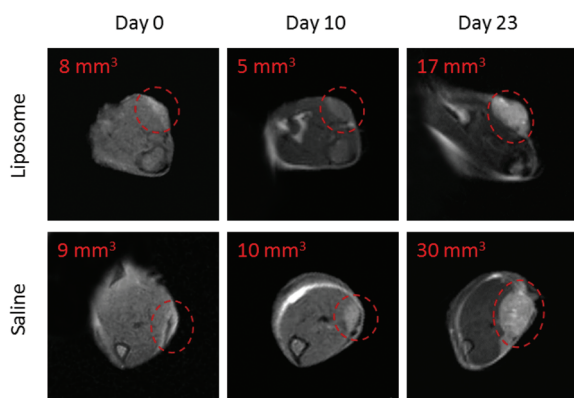


**Fig. 8** *In vivo* antitumor efficiency of RGD-Gd-PTX-L on the A549 implanted mice model assessed by MRI. Tumors were marked by the red dotted line. The tumor volumes were 8, 5, and  $17 \text{ mm}^3$  for the liposome group, and 9, 10,  $30 \text{ mm}^3$  for the control group respectively, at different time points.

and monitoring the tumor development and treatment effect by MRI, potentially in other cancer models.

## Conclusions

In conclusion, lipophilic paclitaxel and hydrophilic Gd-DOTA were successfully assembled into one liposome. c(RGDyk)-modified liposomes can effectively target A549 non-small-cell lung cancer cells *in vitro* and *in vivo*. This delivery system could provide a minimally invasive and real-time MRI strategy with improved sensitivity over non-targeted delivery vehicles. Furthermore, the targeted liposome can effectively target tumor

and tumor microenvironments detectable by a fluorescent technique. The therapeutic effect of this multifunctional liposome provides an exciting avenue to pursue further applications in lung cancer. In addition, integrin is overexpressed in many solid tumor cells and an important target for regulating cancer progression. Therefore, such a peptide-modified liposome may be applicable as carriers in other cancer-related diagnoses and treatment settings.

## Acknowledgements

This work was supported by the Natural Science Foundation of China (81227902, 21305156, 21221064 and 21120102038) and the Chinese Academy of Sciences (KJ CX2-EW-N06-04).

## Notes and references

- 1 T. Tagami, W. D. Foltz, M. J. Ernsting, C. M. Lee, I. F. Tannock, J. P. May and S. D. Li, *Biomaterials*, 2011, **32**, 6570–6578.
- 2 Y. Chen, A. Bose and G. D. Bothun, *ACS Nano*, 2010, **4**, 3215–3221.
- 3 G. Mikhaylov, U. Mikac, A. A. Magaeva, V. I. Itin, E. P. Naiden, I. Psakhye, L. Babes, T. Reinheckel, C. Peters, R. Zeiser, M. Bogyo, V. Turk, S. G. Psakhye, B. Turk and O. Vasiljeva, *Nat. Nanotechnol.*, 2011, **6**, 594–602.
- 4 S. Biswas, N. S. Dodwadkar, P. P. Deshpande and V. P. Torchilin, *J. Controlled Release*, 2012, **159**, 393–402.
- 5 J. Mai, S. Song, M. Rui, D. Liu, Q. Ding, J. Peng and Y. Xu, *J. Controlled Release*, 2009, **139**, 174–181.
- 6 V. P. Chekhonin, V. P. Baklaushev, G. M. Yusubaliev, A. E. Belorusova, M. V. Gulyaev, E. B. Tsitrin, N. F. Grinenko, O. I. Gurina and Y. A. Pirogov, *Nanomed. Nanotechnol.*, 2012, **8**, 63–70.
- 7 L. E. Paulis, I. Jacobs, N. Akker, T. Geelen, D. Molin, L. W. Starmans, K. Nicolay and G. J. Strijkers, *Nanobiotechnol.*, 2012, **10**, 1–12.
- 8 E. Cittadino, M. Ferraretto, E. Torres, A. Maiocchi, B. J. Crielaard, T. Lammers, G. Storm, S. Aime and E. Terreno, *Eur. J. Pharm. Sci.*, 2012, **45**, 436–441.
- 9 T. M. Allen and P. R. Cullis, *Adv. Drug Delivery Rev.*, 2013, **65**, 36–48.
- 10 D. Kozłowska, P. Foran, P. MacMahon, M. J. Shelly, S. Eustace and R. O’Kennedy, *Adv. Drug Delivery Rev.*, 2009, **61**, 1402–1411.
- 11 V. P. Torchilin, *Adv. Drug Delivery Rev.*, 2012, **64**, 302–315.
- 12 Y. Katanasaka, T. Ishii, T. Asai, H. Naitou, N. Maeda, F. Koizumi, S. Miyagawa, N. Ohashi and N. Oku, *Int. J. Cancer*, 2010, **127**, 2685–2698.
- 13 A. Etzerodt, M. B. Maniecki, J. H. Graversen, H. J. Møller, V. P. Torchilin and S. K. Moestrup, *J. Controlled Release*, 2012, **160**, 72–80.

- 14 S. Kaida, H. Cabral, M. Kumagai, A. Kishimura, Y. Terada, M. Sekino, I. Aoki, N. Nishiyama, T. Tani and K. Kataoka, *Cancer Res.*, 2010, **70**, 7031–7041.
- 15 P. G. Tardi, N. D. Santos, T. O. Harasym, S. A. Johnstone, N. Zisman, A. W. Tsang, D. G. Bermudes and L. D. Mayer, *Mol. Cancer Ther.*, 2009, **8**, 2266–2275.
- 16 Y. Liu, W. L. Lu, J. Guo, J. Du, T. Li, J. W. Wu, G. L. Wang, J. C. Wang, X. Zhang and Q. Zhang, *J. Controlled Release*, 2008, **129**, 18–25.
- 17 S. Jain, V. Mishra, P. Singh, P. K. Dubey, D. K. Saraf and S. P. Vyas, *Int. J. Pharm.*, 2003, **261**, 43–55.
- 18 S. Koudelka and J. Turánek, *J. Controlled Release*, 2012, **163**, 322–334.
- 19 K. Na, S. A. Lee, S. H. Jung and B. C. Shin, *Colloids Surf., B*, 2011, **84**, 82–87.
- 20 Y. Liu and N. Zhang, *Biomaterials*, 2012, **33**, 5363–5375.
- 21 M. Tan and Z. Lu, *Theranostics*, 2011, **1**, 83–101.
- 22 Z. Yang, S. G. Kang and R. Zhou, *Nanoscale*, 2014, **6**, 663–677.
- 23 D. Yoo, J. H. Lee, T. H. Shin and J. Cheon, *Acc. Chem. Res.*, 2011, **44**, 863–874.
- 24 C. Li, *Nat. Mater.*, 2014, **13**, 110–115.
- 25 Y. L. Wu, N. Putcha, K. W. Ng, D. T. Leong, C. T. Lim, S. C. J. Loo and X. Chen, *Acc. Chem. Res.*, 2013, **46**, 782–791.
- 26 J. S. Desgrosellier and D. A. Cheresch, *Nat. Rev. Cancer*, 2010, **10**, 9–22.
- 27 Y. Wang, K. Zhou, G. Huang, C. Hensley, X. Huang, X. Ma, T. Zhao, B. D. Sumer, R. J. DeBerardinis and J. Gao, *Nat. Mater.*, 2014, **13**, 204–212.
- 28 L. Zhao, Y. H. Xu, T. Akasaka, S. Abe, N. Komatsu, F. Watari and X. Chen, *Biomaterials*, 2014, **35**, 5393–5406.
- 29 X. Ma, J. Jia, R. Cao, X. Wang and H. Fei, *J. Am. Chem. Soc.*, 2014, **136**, 17734–17737.
- 30 M. Schottelius, B. Laufer, H. Kessler and H. J. Wester, *Acc. Chem. Res.*, 2009, **42**, 969–980.
- 31 G. K. Seward, Y. Bai, N. S. Khan and I. J. Dmochowski, *Chem. Sci.*, 2011, **2**, 1103–1110.
- 32 G. J. Strijkers, E. Kluza, G. A. F. Tilborg, D. W. J. Schaft, A. W. Griffioen, W. J. M. Mulder and K. Nicolay, *Angiogenesis*, 2010, **13**, 161–173.
- 33 R. Haubner, W. A. Weber, A. J. Beer, E. Vabuliene, D. Reim, M. Sarbia, K. F. Becker, M. Goebel, R. Hein, H. J. Wester, H. Kessler and M. Schwaiger, *PLoS Med.*, 2005, **2**, 0244–0252.
- 34 Y. Miura, T. Takenaka, K. Toh, S. Wu, H. Nishihara, M. R. Kano, Y. Ino, T. Nomoto, Y. Matsumoto, H. Koyama, H. Cabral, N. Nishiyama and K. Kataoka, *ACS Nano*, 2013, **7**, 8583–8592.
- 35 S. Xu, B. Z. Olenyuk, C. T. Okamoto and S. F. H. Alvarez, *Adv. Drug Delivery Rev.*, 2013, **65**, 121–138.
- 36 Y. Yoshizawa, K. Ogawara, A. Fushimi, S. Abe, K. Ishikawa, T. Araki, G. Molema, T. Kimura and K. Higaki, *Mol. Pharm.*, 2012, **9**, 3486–3494.
- 37 J. Du, W. L. Lu, X. Ying, Y. Liu, P. Du, W. Tian, Y. Men, J. Guo, Y. Zhang, R. J. Li, J. Zhou, J. N. Lou, J. C. Wang, X. Zhang and Q. Zhang, *Mol. Pharm.*, 2009, **6**, 905–917.
- 38 V. P. Torchilin, *Nat. Rev.*, 2005, **4**, 145–160.
- 39 P. Crosasso, M. Ceruti, P. Brusa, S. Arpicco, F. Dosio and L. Cattel, *J. Controlled Release*, 2000, **63**, 19–30.
- 40 M. Hossann, T. Wang, Z. Syunyaeva, M. Wiggenhorn, A. Zengerle, R. D. Issels, M. Reiser, L. H. Lindner and M. Peller, *J. Controlled Release*, 2013, **166**, 22–29.
- 41 S. Meng, B. Su, W. Li, Y. Ding, L. Tang, W. Zhou, Y. Song, H. Li and C. Zhou, *Nanotechnology*, 2010, **21**, 1–7.
- 42 J. A. Zhang, G. Anyarambhatla, L. Ma, S. Ugwu, T. Xuan, T. Sardone and I. Ahmad, *Eur. J. Pharm. Biopharm.*, 2005, **59**, 177–187.
- 43 A. Sharma, E. Mayhew, L. Bolcsak, C. Cavanaugh, P. Harmon, A. Janoff and R. J. Bernacki, *Int. J. Cancer*, 1997, **71**, 103–107.
- 44 P. Ma and R. J. Mumper, *J. Nanomed. Nanotechnol.*, 2013, **4**, 1–16.
- 45 V. P. Chauhan and R. K. Jain, *Nat. Mater.*, 2013, **12**, 958–962.